Evaluation of Different Mapping Techniques for the Integration of Electro-Anatomical Voltage and Imaging Data of the Left Ventricle

David Soto-Iglesias[1,⋆], Constantine Butakoff[1], David Andreu[2], Juan Fernández-Armenta[2], Antonio Berruezo[2], and Oscar Camara[1]

[1] PhySense, DTIC, Universitat Pompeu Fabra, Barcelona, Spain,
[2] Arrhythmia Section, Cardiology Department, Thorax Institute, Hospital Clinic, Barcelona, Spain
david.soto@upf.edu

Abstract. Integration of electrical and structural information about substrate in the left ventricle is very important to guide ablation therapies in ventricular tachycardia cases. This integration asks for finding a mapping between electro-anatomical voltage mapping and delay-enhancement magnetic resonance images. We present an evaluation of the accuracy of some mapping strategies, including different standard rigid and non-rigid registration techniques. We also developed a new mapping algorithm to be applied once both geometries are roughly aligned to improve the currently used simple closest point projection. The new mapping algorithm is based on establishing a homeomorphism between both surfaces using a common surface parametrization computed by mesh flattening, then preserving all original information in both modalities. We applied the different mapping strategies to clinical and synthetic data. Results demonstrated a substantial reduction of the point-to-surface error when using the non-rigid registration technique and an improved substrate overlap when using the proposed mapping algorithm.

Keywords: registration, electro-anatomical voltage mapping, MRI, cardiac arrhythmias.

1 Introduction

Normally the treatment protocol of Ventricular tachycardia (VT), one of the commonest forms of arrhythmia, starts with anti-arrhythmic drugs and if no improvement is observed radio-frequency ablation (RFA) is performed. RFA aims at detecting and eliminating electrical conduction pathways within myocardial substrate that are responsible for the VT and are generally guided by electro-anatomical voltage mapping (EAVM) that produces a set of sparse acquisition points where local electrical activity is obtained. This information is crucial to identify potential ablation targets but there is still a low success ratio of these interventions (e.g. recurrence rates up to 91% [1] in some patients) and ablated areas could be substantially reduced with further insight on tissue heterogeneity.

⋆ Corresponding author.

S. Ourselin, D. Rueckert, and N. Smith (Eds.): FIMH 2013, LNCS 7945, pp. 391–399, 2013.

In the last few years, more specific ablation strategies have been developed for scar-related VTs such as the so-called dechannelling technique [1] that targets the slow conduction zones inside the scar (conduction channels, CC). Nevertheless, identifying CCs exclusively from EAVM requires considerable operator experience, suffers from substantial inter- and intra-observer variability and it is highly time-consuming. Recently, structural 3D information of scar tissue characteristics obtained from processing delay-enhancement magnetic resonance images (de-MRI) have been incorporated into the VT therapy planning ([2] among others), helping to better identify CCs when integrated with electrical information given by EAVMs.

The integration of EAVM and de-MRI information requires computing the mapping between both reference systems, which is a non-trivial task since anatomical information provided by EAVM is not very accurate and data acquisition is performed in different patient's conditions. The mapping between EAVM and de-MRI can be guided by a set of anatomical landmarks identified in both modalities, whereupon a transformation is estimated. Simple rigid transformations are the most commonly used in clinical routine since the CARTO system (CARTO, Biosense, Cordis Webster, Marlton, NJ) includes a software (CartoMerge) optimizing both point-to-surface distance and landmark alignment [3]. Rigid transformations, however may not sufficiently accurate due to deformations between EAVM and de-MRI data induced by having different sampling, spatial resolution and inaccuracies in EAVM anatomical information. Some authors [4,5] have included scar information to further constrain rigid transformations between EAVM and de-MRI data but they are strongly dependent on the scar definition in both modalities, which highly depends on the thresholds employed to classify scar tissue types [2].

In this work we evaluate different mapping techniques to integrate EAVM and de-MRI derived information of the left ventricle (LV) on a set of synthetically generated ground-truth data with varying characteristics and on clinical data. Standard landmark-based rigid transformations and well-known non-rigid shape registration techniques are compared regionally. In addition, we present and evaluate a new mapping technique that establishes a homeomorphism between EAVM and de-MRI LV geometries using a common surface parameterization calculated by mesh flattening and it is compared to the currently used simple closest point mapping method (CP).

2 Clinical and Synthetic Data

2.1 Clinical Data

In this work we applied different mapping techniques on data available for 9 patients with different scar configuration (6 ischemic with mostly sub-endocardial scars and 3 non-ischemic with mostly transmural scars) that underwent VT ablation. EAVM acquired with a CARTO system and de-MRI were available for all of them.

Endocardial contact mapping data was collected with a CARTO 3 system after introducing a quadripolar catheter through the femoral vein until reaching the endocardium. EAVMs were subsequently generated by reconstructing information obtained from the set of sparse acquisition points where the clinician placed the catheter to measure the electrical activity (around 2500ms at 1kHz). The electrical measurements were processed and rendered in 3D to display relevant information such Local Activation Time (LAT) or maximum bipolar (BIP) maps where tissue heterogeneous regions were easily identified. In this study, the average number of acquired CARTO points for each patient was 410±242, with a non-homogeneous distribution since more than half of these points were placed in scar-related areas.

All subjects underwent de-MRI examination before the VT ablation procedure using a 3T clinical scanner (Magnetom Trio, Siemens Healthcare). The 3D slab was acquired in the transaxial direction, with a 256×256 pixels matrix size and minimized field of view. The acquired voxel size was adjusted to achieve an isotropic spatial resolution of 1.4×1.4×1.4 mm, giving a set of (typically 50-70 images) images in the LV short-axis orientation.

2.2 Generation of Synthetic Data

The synthetic datasets of corresponding de-MRI and EAVM surfaces were generated from de-MRI endocardial surfaces of two different patients (one with small scar and one with large scar). Each of the surfaces was transformed by a random rigid transformation with translation of up to 10mm and rotation of up to ±1rad as in [5]. To simulate the different resolutions of EAVM, 300, 400, 500, 600 vertices were randomly sampled from the de-MRI mesh making sure that 50% of them lie in the scar. Finally, a Gaussian noise of standard deviation $\sigma = 1$ and $\sigma = 3$ (as in [5]) was added to the vertex coordinates along the surface normal (maximum possible point displacement will be on the order of 9mm) to simulate uncertainties in EAVM point localizations and imperfect catheter contact. An example can be seen in the second column of Fig. 1.

3 Methods

3.1 Segmentation of Ventricular Geometry and Substrate

LV geometry was extracted from de-MRI using a segmentation algorithm based on guiding the alignment of atlas-based information with manual landmarks [6]. Once the whole myocardium of the LV was obtained, we divided it into 5 layers from the endocardium to the epicardium (10%, 25%, 50%, 75%, 90% from the endocardium) and projected the de-MRI pixel intensities to better study scar characteristics (e.g. transmurality), as in [2].

Cardiac tissue can be separated into three types: core zone (CZ, non-conducting scarred tissue); border zone (BZ, area surrounding the scar with some low levels of conductivity); and healthy tissue (HT). This tissue characterization is extremely important for VTs and is usually performed both in de-MRI

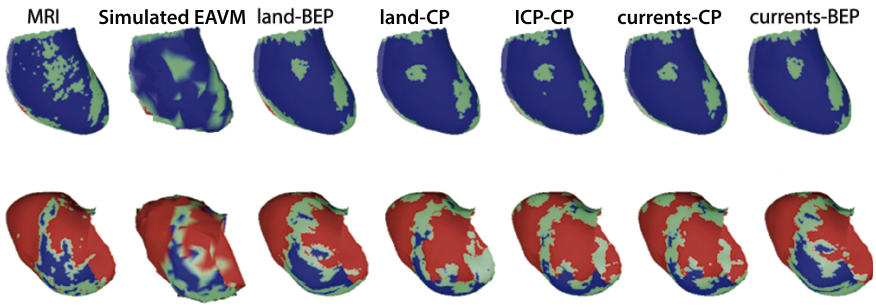

Fig. 1. Synthetic datasets. Top row – large scar, bottom row – small scar. Colours correspond to different zones: core zone(CZ) in blue, border zone (BZ) in green and healthy tissue (HT) in red.

and in EAVMs. For identifying the CZ, BZ and HT in de-MRI, some thresholds were applied on the set of pixel intensities based on the maximum intensity point (MIP), as proposed in [2]: for a pixel intensity i, if $i \geq 60\%$ of the MIP, i is classified as CZ; for $i < 40\%$ of the MIP, i is identified as HT; otherwise ($40\% < i \leq 60\%$ of the MIP), i is labelled as BZ. Using these thresholds, the average percentage of scar (CZ+BZ) with respect to the LV mass (tissue volume), computed as the percentage of scar vs total nodes in the LV mesh, was of 48.64±20.84.

BIP maps, are computed as the maximum amplitude of the electrical signal for each point, are currently used to characterize scar distribution in EAVMs, where lower electrical activity is expected in scar areas. The standard threshold values to identify CZ, BZ and HT from BIP values (j) are the following (see [2] for further details): $j \geq 1.5$mV correspond to HT; $j < 0.5$mV are classified at CZ; otherwise ($0.5\text{mV} \leq j \leq 1.5\text{mV}$) these values are BZ. One drawback of this characterization in EAVMs is that BIPs are corrupted by far-field effect produced by healthy tissue surrounding the scar zone, not necessarily in the endocardium. For this reason, we took into account the three first layers in de-MRI (average of 10%, 25%, 50% from endocardium) when comparing it to EAVM scar distribution. Using these thresholds, the average percentage of scar (CZ+BZ) with respect to the LV mass found in EAVMs was of 32.81±12.20.

3.2 Registration Techniques

In order to perform the mapping between EAVM and de-MRI information, LV geometries from both modalities need to be aligned. This alignment has been carried out using three commonly used registration approaches. The landmark-based registration estimates a rigid transformation between two surfaces based on a set of manually placed landmarks, in our case 7 landmarks selected in both surfaces (6 in the mitral annulus, one in the apex). The resulting rigid transformation is used to initialize more advanced registration techniques. Due to the

symmetry of LV it is possible to register any two LV surfaces only up to a rotation angle about the long axis (LA), then the iterative closest point (ICP) [7], which iteratively estimates the rigid transformation based on the distance between the points of the two surfaces, is also tested. Finally the non-rigid currents-based registration [8] is evaluated due to its flexibility in aligning complex surfaces in different computer vision applications.

3.3 Electro-Anatomical Voltage Mapping

Two methods for mapping EAVM data to the de-MRI mesh will be used. The de-MRI mesh is taken as a reference for mapping due to a much higher accuracy of anatomy reconstruction as compared to EAVM.

Mapping by Finding the Closest Point (CP). This method is the simplest one to project information from the registered EAVM mesh to the de-MRI geometry. Given two registered meshes, for every vertex of de-MRI mesh, we look up the closest face of the EAVM mesh and the closest point within this face together with its barycentric coordinates. Using the barycentric coordinates the values of BIP of the face vertices are interpolated and the result is associated to the original de-MRI vertex.

Mapping through a Homeomorphism between Surfaces (HM). The endocardial surfaces have a form of a cut ellipsoid and are homeomorphic to a disk. This homeomorphism can be calculated by requiring that every vertex coordinate of the triangulation has a vanishing Laplacian. By mapping both de-MRI and EAVM surfaces to the same disk we can easily establish a piecewise linear homeomorphism between the two surfaces [9,10]. This methodology provides a simple method for mapping surfaces with one hole to a unit disk, where the edge of the surface is mapped to the circumference of the disk, with the imposed constraint of preserving the relative distance between the points of the edge. However, since we will use the disk to establish a mapping between two endocardial surfaces, the cardiac apex of one surface needs to be mapped to the apex of the other one. We will enforce this constraint by mapping the apex to the center of the disk. This can be achieved by applying thin-plate splines (TPS) to displace the apical point to the center after flattening, while uniformly spreading the deformation to all the cells. Once we know the mapping $\varphi_{de-mri\to D}$ from the de-MRI surface to the disk and $\varphi_{eavm\to D}$ from the EAVM surface to the disk, both can be thought of as two triangulations of the same disk. At this point, $\varphi^{-1}_{de-mri\to D}\cdot\varphi_{eavm\to D}$ can be used to map any scalar field from the EAVM surface to the de-MRI surface. The procedure is as follows. Let $(\mathbf{x}_{eavm\to D}, \mathbf{y}_{eavm\to D})$ and $(\mathbf{x}_{de-mri\to D}, \mathbf{y}_{de-mri\to D})$ be the vertices of the EAVM and de-MRI, respectively, projected onto the disk. Construct the matrix $\mathbf{T}$ expressing every point $(\mathbf{x}_{de-mri\to D}, \mathbf{y}_{de-mri\to D})$ in terms of barycentric coordinates of the triangulation of $(\mathbf{x}_{eavm\to D}, \mathbf{y}_{eavm\to D})$. Let $\mathbf{c}_{eavm}$ be some scalars

Table 1. Correlation (Correl) and Dice values (mean%±STD%) averaged over different configurations of small and large scar synthetic data provided by the different mapping techniques: landmarks (land-), ICP and currents (curr) with closest point (CP) or mapping through a homeomorphism (HM) mappings. CZ: core zone; BZ: border zone; HT: healthy tissue.

	Small scar				Large scar			
	Correl	Dice			Correl	Dice		
		CZ	BZ	HT		CZ	BZ	HT
land-CP	0.59±0.15	0.24±0.13	0.22±0.07	0.72±0.06	0.73±0.14	0.63±0.09	0.33±0.10	0.52±0.14
ICP-CP	0.67±0.13	0.33±0.13	0.26±0.07	0.75±0.05	0.79±0.11	0.65±0.08	0.37±0.12	0.59±0.12
curr-CP	0.69±0.12	0.33±0.13	0.26±0.06	0.75±0.04	0.80±0.10	0.66±0.08	0.38±0.12	0.60±0.11
land-HM	0.74±0.07	0.35±0.05	0.27±0.06	0.76±0.04	0.82±0.07	0.66±0.07	0.38±0.09	0.60±0.08
curr-HM	0.75±0.07	0.37±0.05	0.27±0.06	0.76±0.04	0.80±0.07	0.65±0.06	0.36±0.08	0.58±0.09

associated to the vertices of EAVM mesh. Then the corresponding scalars on the de-MRI mesh can be computed by

$$\mathbf{c}_{eavm \to de-mri} = \mathbf{T} \cdot \mathbf{c}_{eavm} \tag{1}$$

As mentioned above, besides the apex, one point has to be selected on the edge of the mesh ∂M for both surfaces. This point is located in the middle of the septum. ∂M coincides with the mitral annulus (MA). The selected point is mapped to the point (-1,0) of the ∂D.

4 Results

Registration Accuracy. First of all, registration accuracy was evaluated on the synthetic and patient datasets computing the point-to-surface average distance between the EAVM (points) and the de-MRI (surfaces). The average distances for synthetic datasets were: 1) landmarks – 3.59±0.94mm; 2) ICP – 2.12±0.85mm; 3) currents – 1.14±0.46mm; This registration error is acceptable considering the amount of noise added to the synthetic datashet (maximum displacement of around 9mm). The average registration errors for patient datasets were: 1) landmarks – 6.68±5.25mm; 2) ICP – 4.25±3.04mm; 3) currents – 0.97±0.97mm. Registration errors obtained with rigid transformations are in the same order to those recently published [4,5].

Mapping Accuracy. The mapping accuracy was evaluated by comparing how well the scar information from EAVM was aligned with that from de-MRI. The values were analyzed at the vertices of the de-MRI mesh. Prior to comparison the voltage and intensity values were classified into HT, BZ, CZ as defined in Section 3.1. The comparison is carried out computing the correlation between original EAVM and de-MRI values and the Dice coefficient between the labels obtained after thresholding. Results are summarized in Table 1 and Table 2. It should be noted that the Dice values obtained are in the same range to those

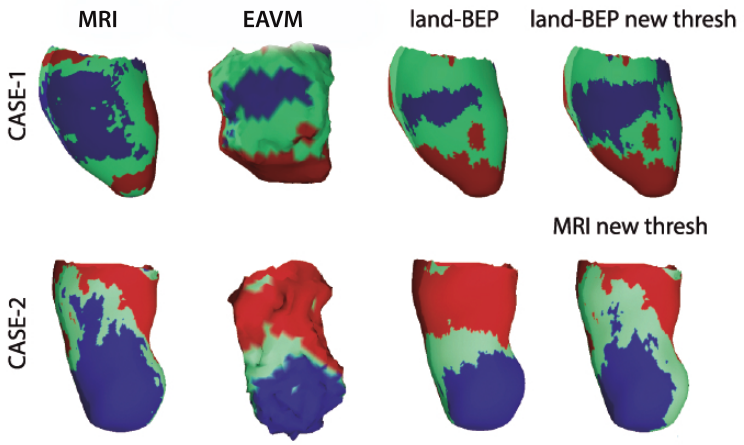

Fig. 2. Two clinical datasets: first three columns show scar labels using standard MIP-based thresholds, fourth topmost figure is land-HM (HM after landmark-based registration) with threshold 0.8-1.5mV and fourth down figure MRI threshold 40%-70% MIP (see discussion). Core zone (CZ) in blue, border zone (BZ) in green and healthy tissue (HT) in red.

obtained when comparing scar segmentation techniques with manually obtained ground-truth in the de-MRI challenge recently organized at STACOM'12[1].

5 Discussion and Conclusions

Synthetic Datasets. In this paper several mapping strategies were compared using different registration techniques combined with different mapping techniques. As can be seen in Table 1 the ICP-based mapping performs better than the landmarks one. The mapping after the currents method is slightly better than those of ICP due to a more accurate registration. On the other hand HM results are consistently better than CP ones, especially in the case of small scar configuration where HM mapping preserves better more heterogeneous structures. An interesting observation can be made by noticing that applying HM mapping after currents does not improve the accuracy of HM mapping after a simple landmark based registration. This can be explained by the fact that in principle HM relies only on the position of two landmarks and is independent of the alignment of the two surfaces, however it should be noted that currents deforms the mesh, changing the produced mapping as a consequence.

Patient Datasets. It can be seen from Fig. 2 that even though there is a clear relation between observed structures in de-MRI and EAVM datasets, there are also large differences due to the different nature of observed measurements.

[1] `http://www.physense.org/stacom2012`

Table 2. Correlation (Correl) and Dice values (mean%±STD%) averaged over 9 different cases provided by the different mapping techniques: landmarks (land-), ICP and currents (curr) with closest point (CP) or mapping through a homeomorphism (HM) projection. CZ: core zone; BZ: border zone; HT: healthy tissue.

	Correl	Dice		
		CZ	BZ	HT
land-CP	0.35±0.15	0.17±0.11	0.18±0.09	0.50±0.13
ICP-CP	0.32±0.13	0.19±0.13	0.19±0.08	0.52±0.16
curr-CP	0.37±0.10	0.18±0.12	0.20±0.09	0.51±0.16
land-HM	0.39±0.09	0.18±0.11	0.22±0.10	0.50±0.15
curr-HM	0.38±0.09	0.19±0.12	0.21±0.09	0.52±0.14

These differences can significantly hamper the evaluation. The thresholds proposed in [2] may not be optimal for all cases, as can be observed in Fig. 2 (4th column compared to 1st column), where thresholds are slightly changed and better overlap between EAVM and de-MRI data is obtained. This situation produce lower correlation and Dice scores as compared to the synthetics ones. However, in Table 2 one can observe that HM is still consistently better than CP.

General Remarks. In this work we have demonstrated that HM mapping without advanced registration techniques is better or comparable to that of CP combined with registration techniques, however there is an added benefit of not losing small structures such as CCs. This is closely related to the way the mapping is computed, which makes sure that all the faces of the EAVM mesh get mapped onto the de-MRI surface, while CP is dependent on the angle the face has to the de-MRI surface. However if an accurate non-rigid registration technique is available, it can be used to correct the initial landmark positions, improving the overall accuracy of the mapping. Once EAVM and de-MRI information are integrated, we plan to detect subtle structures such as conduction channels jointly using data in both modalities. Future work will also focus on developing new benchmark scenarios to better identify influencing factors for the accuracy of the mapping such as different scar characteristics, landmarks inaccuracies or number of EAVM points.

Acknowledgments. This study was partially founded by Spanish Ministry of Science and Innovation (TIN2011-28067).OC acknowledges grant support from the Spanish MEC under the program ISCIII(FIS-PI11/01709)

References

1. Berruezo, A., Fernández-Armenta, J., Mont, L., Zeljko, H., Andreu, D., Herczku, C., Boussy, T., Tolosana, J.M., Arbelo, E., Brugada, J.: Combined endocardial and epicardial catheter ablation in arrhythmogenic right ventricular dysplasia incorporating scar dechanneling technique. Circulation: Arrhythmia and Electrophysiology 5(1), 111–121 (2012)

2. Andreu, D., Berruezo, A., Ortiz-Pérez, J., Silva, E., Mont, L., Borràs, R., de Caralt, T., Perea, R., Fernández-Armenta, J., Zeljko, H., Brugada, J.: Integration of 3D electroanatomic maps and magnetic resonance scar characterization into the navigation system to guide ventricular tachycardia ablation. Circulation: Arrhythmia and Electrophysiology 4(5), 674–683 (2011)
3. Li-Fern, H.: Image integration for catheter ablation: searching for the perfect match. Heart Rhythm 5(4), 536–537 (2008)
4. Tao, Q., Milles, J., Van Huls Van Taxis, C., et al.: Toward magnetic resonance-guided electroanatomical voltage mapping for catheter ablation of scar-related ventricular tachycardia: A comparison of registration methods. Journal of Cardiovascular Electrophysiology 23(1), 74–80 (2012)
5. Roujol, S., Basha, T., et al.: Improved multi-modality data fusion of late gadolinium enhancement MRI to left ventricular voltage maps in ventricular tachycardia ablation. IEEE Transactions on Biomedical Engineering (2012) (in press)
6. Tobon-Gomez, C., Sukno, F., Butakoff, C., Huguet, M., Frangi, A.: Automatic training and reliability estimation for 3D ASM applied to cardiac MRI segmentation. Physics in Medicine and Biology 57(13), 41–55 (2012)
7. Besl, P., McKay, H.: A method for registration of 3-d shapes. IEEE Transactions on Pattern Analysis and Machine Intelligence 14(2), 239–256 (1992)
8. Vaillant, M., Glaunès, J.: Surface matching via currents. In: Christensen, G.E., Sonka, M. (eds.) IPMI 2005. LNCS, vol. 3565, pp. 381–392. Springer, Heidelberg (2005)
9. De Craene, M., Tobon-Gomez, C., Butakoff, C., Duchateau, N., Piella, G., Rhode, K.S., Frangi, A.F.: Temporal diffeomorphic free form deformation (TDFFD) applied to motion and deformation quantification of tagged MRI sequences. In: Camara, O., Konukoglu, E., Pop, M., Rhode, K., Sermesant, M., Young, A. (eds.) STACOM 2011. LNCS, vol. 7085, pp. 68–77. Springer, Heidelberg (2012)
10. Tutte, W.: How to draw a graph. Proceedings of the London Mathematical Society 13(3), 743–768 (1963)